



HHS Public Access

Author manuscript

Oncogene. Author manuscript; available in PMC 2014 January 11.

Published in final edited form as:

Oncogene. 2013 July 11; 32(28): 3359–3370. doi:10.1038/onc.2012.352.

Histone Methylase MLL1 plays critical roles in tumor growth and angiogenesis and its knockdown suppresses tumor growth *in vivo*

Khairul I. Ansari, Sahba Kasiri, and Subhrangsu S. Mandal*

Department of Chemistry and Biochemistry The University of Texas at Arlington Arlington, Texas 76019

Abstract

Mixed lineage leukemias (MLL) are human histone H3 lysine-4 specific methyl transferases that play critical roles in gene expression, epigenetics, and cancer. Herein, we demonstrated that antisense-mediated knockdown of MLL1 induced cell cycle arrest and apoptosis in cultured cells. Intriguingly, application of MLL1-antisense specifically knocked down MLL1 *in vivo* and suppressed the growth of xenografted cervical tumor implanted in nude mouse. MLL1-knockdown downregulated various growth and angiogenic factors such as HIF1 α , VEGF and CD31 in tumor tissue affecting tumor growth. MLL1 is overexpressed along the line of vascular network and localized adjacent to endothelial cell layer expressing CD31, indicating potential roles of MLL1 in vasculogenesis. MLL1 is also overexpressed in the hypoxic regions along with HIF1 α . Overall, our studies demonstrated that MLL1 is a key player in hypoxia signaling, vasculogenesis, and tumor growth, and its depletion suppresses tumor growth *in vivo*, indicating its potential in novel cancer therapy.

Introduction

Understanding the tumor microenvironment and the signaling mechanism that controls tumor growth, angiogenesis, and metastasis, is critical for developing novel and effective cancer therapy. Abnormal expression of various transcription factors has been implicated in tumorigenesis and they are potential targets for novel cancer therapy (1-4). For example, epidermal growth factor receptor (EGFR) and vascular endothelial growth factor receptor (VEGFR), which are overexpressed in variety of cancers, are being targeted for developing cancer therapy (5, 6). Histone modifying enzymes that are key players in gene regulation and epigenetics are found to be misregulated in variety of tumors and therefore provides novel platform for understanding the tumor biology as well as developing potential targeted therapy (7-11).

Mixed lineage leukemias (MLL) are human histone H3 lysine-4 (H3K4) specific methyltransferases (HMTs) that play critical roles in gene expression (12-24). In human,

Users may view, print, copy, download and text and data- mine the content in such documents, for the purposes of academic research, subject always to the full Conditions of use: http://www.nature.com/authors/editorial_policies/license.html#terms

*To whom correspondence should be addressed. Tel: 817-272-3804, Fax: 817-272-3808, smandal@uta.edu.

there are several MLL families of proteins that include MLL1, MLL2, MLL3, MLL4, Set1 etc. MLLs are well-known for their association with oncogenic transformation (13, 18, 25, 26). MLL1 is often rearranged in acute lymphoblastic and myeloid leukemias in children and adults (13, 18, 25). MLL2-4 are mutated or misregulated in various solid tumors (27-33). MLLs are also well known as master regulators of homeobox (HOX) genes that are critical players during cell differentiation and embryonic development. MLLs (MLL1-4) exist as multi-protein complexes inside cell, with several common subunits that include Ash2, Wdr5, Rbbp5, Dpy30 and CGBP (26, 34, 35). The distinct cellular functions of different MLLs as well as their interacting proteins still remain elusive. Studies from our laboratory and others showed that MLL1 is a key player in cell cycle progression and stress-response (21, 26, 36-38). Depletion of MLL1 results in cell cycle arrest at G2/M phase (21, 39). MLLs also participate in steroid hormone-mediated gene regulation and signaling, indicating their potential association with hormone-linked diseases including breast and prostate cancer (26, 40-42). Although, a great deal of efforts are being invested towards understanding the functions of MLL-histone methylases in gene regulation and disease, their therapeutic potential remain mostly unexplored.

To understand the roles of MLL-histone methylases in tumor cell signaling and explore their therapeutic potential, we knocked down MLL1 in different cultured tumor cells and also in mice and examined its impact on cell viability, cell cycle progression and on tumor growth *in vivo*. Our results demonstrated that MLL1 plays critical roles in cell cycle progression. Importantly, knockdown of MLL1 induced apoptosis in cultured tumor cells and suppressed the growth of xenografted tumor *in vivo* (xenografted tumor model). MLL1 is also associated with angiogenesis and hypoxia signaling.

Results and discussion

MLL1 is essential for cell viability and its depletion induces apoptosis in cultured mammalian cells

To investigate the importance of MLL1 in cell survival and maintenance, we knocked it down in different malignant and nonmalignant cultured human cell lines using MLL1-specific phosphorothioate antisense oligonucleotide and examined its impact on cell viability. Initially, we screened five different MLL1-antisenses (MLL1-A1 to MLL1-A5, **Table S1, Fig. S1**) to examine their knockdown efficacy and specificities in HeLa cells. MLL1-A3 and MLL1-A5 antisenses showed the most effective MLL1-knockdown in comparison to other antisenses examined (Fig. S1b-f), MLL1-A3 showed slightly higher knockdown efficacy than MLL1-A5 (Fig. S1b-f), As MLL1-A3 was the most effective antisense, it was used for all the remaining studies and it is termed as MLL1-antisense throughout this manuscript. To examine the efficacy of the antisenses, we transfected HeLa cells with varying concentrations (3-7 μ g) of MLL1-specific and scramble (that has no homology to MLL1) antisenses (**Table S1**) and incubated for 48 h. Our analysis demonstrated that MLL1-antisense efficiently knocked down MLL1 both at the protein and mRNA level (compare lanes 3-5 with lane 1, **Figs. 1a and b**). The level of MLL2 (control) was mostly unaffected upon MLL1-knockdown (**Figs. 1a and b**). The scramble antisense

had no significant effect on MLL1 expression (lane 2, **Figs. 1a** and **b**). These results demonstrated that MLL1-antisense specifically knocked down MLL1 in HeLa cells.

To examine the effects of MLL1-knockdown on cell viability, we transfected the MLL1 antisense (7 μ g) to different malignant and nonmalignant cells and then visualized the cell morphology under microscope and also quantified the cell viability using MTT assay (**Figs. 1c** and **d**). The knockdown efficiencies of MLL1 in different cell lines are shown in the supplementary figure **S2**. Microscopic analysis showed that scramble antisense has no significant effects on cellular morphology and growth in most cell types (**Fig. 1c**). The growth and morphology of HeLa, H358 (lung cancer), SW480 (colon cancer), MCF7 (human breast cancer), and JAR (human placenta choriocarcinoma) cells were severely affected upon MLL1-knockdown (**Fig. 1c**). Cells were arrested, rounded up and degenerated. MTT assay showed that HeLa cells were the most sensitive (>90 % cell death) to MLL1-knockdown (**Fig. 1d**). Breast cancer cells (MCF7, 50 % cell death) were slightly more sensitive than normal breast cells (MCF10, 22% death) (**Fig. 1d**). Lung cancer and placenta choriocarcinoma cells were also killed upon MLL1-knockdown. As HeLa cells were most sensitive towards MLL1-knockdown, we performed all the following experiments using this cell line.

To understand the nature of cell death upon MLL1-knockdown, we performed various apoptosis assays. TUNEL assay confirmed that MLL1-knockdown induced apoptosis in HeLa cells (**Fig. 1e**). Briefly, cells were transfected with MLL1-antisense for 48 h and then subjected to DAPI staining, end-labeling of the nicked DNA with fluorescent dUTP (TUNEL assay) and propidium iodide (PI) staining. Analysis of DAPI-stained cells showed that MLL1-antisense induced nuclear condensation (intense DAPI staining) and fragmentation of cell nuclei (condensation and fragmentations are shown by arrows, **Fig. 1e**). Fluorescent dUTP end-labeling demonstrated that cell nuclei were fragmented upon MLL1-antisense treatment (green colored nuclei in MLL1-antisense-treated cells, dUTP panels in Fig. 1e). PI (another DNA binding fluorescent dye that stains dead cells) staining demonstrated that all the cells that were stained green in dUTP staining were co-localized with red (dead) cells (PI staining, **Fig. 1e**). These observations demonstrated that MLL1-knockdown induced apoptosis in HeLa cells. MLL1-knockdown also induced release of cytochrome-c from the mitochondria to cytosol and also induced caspase3/7 activity (**Fig. S3**). We also performed the apoptosis assays (TUNEL and caspase assays) on two nonmalignant cell lines (MCF10 and CCD-18Co) that showed relatively less sensitivity towards MLL1-knockdown (as seen in Figs. 1c-d). TUNEL and caspase analysis showed that MLL1-knockdown induced relatively lesser degree of nuclear fragmentation, caspase 3/7 activation, and apoptotic cell death in both MCF10 and CCD-18Co than HeLa cells, indicating higher sensitivity of malignant cells towards MLL1-knockdown (**Figs. S4a-d** and **Fig 1c-d**).

To rule out the potential off target effect of MLL1-antisense (MLL1-A3), we examined the impact of MLL1-knockdown using another MLL1-antisense (MLL1-A5, Table S1) on cell viability. Our analysis showed that transfection with MLL1-A5 also effectively knocked down MLL1 level in HeLa cells without affecting MLL2 expression (Fig S5a). MLL1-A5-mediated MLL1-knockdown affected cell viability (MTT assay and microscopic images are

shown in Figs. S5b-c), induced nuclear fragmentation (TUNEL assay, Fig S5d) and caspase 3/7 activation (Fig S5e), indicating apoptotic cell death. These studies further demonstrated that knockdown of MLL1 induced apoptosis in cultured cells indicating critical roles of MLL1 in cell viability.

MLL1 is critical player in cell cycle progression

As MLL1 showed essential roles in cell viability, we examined its potential mode of action. We knocked down MLL1 in HeLa cells using specific antisense-oligonucleotide and analyzed its impact on cell cycle progression. We transfected HeLa cells with MLL1 or scramble-antisense for varying time periods, stained with propidium iodide and analyzed by flow cytometry. Upon application of the MLL1-antisense, even at 48 h post treatment, the cell population at G0/G1 phase was decreased dramatically from 72.5 % to 40.3%, while G2/M phase cell population was increased from 13.6 to 35.1% indicating potential cell cycle arrest at G2/M phase. At 24 h post-antisense treatment, 24 % cells underwent apoptosis (**Fig. 2a**). Longer time incubation with MLL1-antisense increased apoptotic cell population (61% at 72 h) while cell populations at G0/G1 and G2/M phases were decreased (**Fig. 2a**). Scramble-antisense showed no significant impact on cell cycle progression. These results demonstrated that MLL1-knockdown induced G2/M phase cell cycle arrest and apoptosis in HeLa cells.

As MLL1-knockdown induced cell cycle arrest, we examined the effect of knockdown on various cell cycle regulatory genes (21, 43). We analyzed RNA from MLL1-antisense treated and control cells by using RT-PCR and quantitative PCR (qPCR). Our results showed that MLL1-knockdown down-regulated the expression of various cell cycle regulatory genes such as cyclin A, cyclin B and p57 (**Fig. 2b**, qPCR data is in the right panel). Chromatin immuno-precipitation (ChIP) studies showed that MLL1-knockdown resulted in decreased histone H3K4-trimethylation and RNA polymerase II (RNAPII) recruitment at the promoters of cyclin A, cyclin B and p57 affecting their expression (**Fig. 2c**). These results demonstrated that MLL1 is a key regulator of cyclins and p-proteins and hence regulate cell cycle progression.

Notably, cell cycle progression is tightly regulated by sequential activation and inactivation of various cyclin-dependent kinases (Cdks) whose activities are regulated by cyclins (44, 45). The cyclin D and E are required for progression through G1 phase. Cyclin A is produced in late G1 and it accumulates during S and G2 phase. The cyclin B is typically expressed during the G2 to M phase transition and controls passage through the M phase (44, 45). Our results showed that knockdown of MLL1 down-regulated the cyclin B expression while cyclin D and E are mostly unaffected (**Fig. 2b**). As cyclin B is critical for G2 to M phase transition, down-regulation of cyclin B under MLL1-knockdown environment contributed towards cell cycle arrest at G2/M phase (Fig 2a). We also observed that MLL1-knockdown down regulated p57 expression. Notably, p57 is well recognized as CDK inhibitor and its inhibition increases cell proliferation (46). Thus, the decrease in p57 upon MLL1-knockdown should increase cell proliferation, instead of observed apoptosis. However, as cyclin B and p57 are common targets of MLL1, it is likely that the effect of G2/M phase arrest via cyclin B down regulation may have surpassed the proliferative effect

of p57 down-regulation under MLL1-knockdown environment. These analyses demonstrated that MLL1 is a critical player in cell cycle regulation and its knockdown resulted in G2/M phase cell cycle arrest, ultimately leading to apoptosis.

MLL1-knockdown suppressed cervical tumor growth in vivo

As MLL1-knockdown induced apoptosis in HeLa cells, we explored potential impact of MLL1-knockdown in controlling cervical tumor growth *in vivo* using mouse xenograft model. Prior to getting into xenograft experiments, we examined the animal toxicity of MLL1-antisense using athymic nude mouse. We injected intraperitoneally three different doses (100, 300 and 500 $\mu\text{g}/20$ gm body weight) of MLL1-antisense (MLL1-A3) and scramble antisense into six weeks old nude mouse (3 replicates each) and then monitored the health of each mouse on a daily basis for a month. Notably, similar ranges of antisense doses are known to be effective in anti-neoplastic therapy (2). Our results demonstrated that upon application of MLL1-antisense, all mice survived without loss of body weight and grown similar to untreated control mice.

As MLL1-antisense showed no significant toxicity towards mouse, we examined its efficacy towards regression of cervical cancer xenograft implanted in nude mouse. We administered MLL1-antisense intraperitoneally on athymic nude mice carrying the cervical cancer xenografts. In brief, 2×10^6 human cervical cancer cells (HeLa cells in 100 μl of PBS) were injected subcutaneously (near the right back limb). Animals were examined daily for signs of tumor growth and behavior. Once the tumor size reached ~ 30 mm² (2 to 3 weeks after injection of HeLa cells), we administered MLL1-antisense intraperitoneally (in PBS, at four days intervals, 300 $\mu\text{g}/20$ gm body weight, in three parallel replicates). To administer the antisense systemically, we injected antisense near the rear left limb of the mice which is away from the tumor area. Control mice were injected with equal volume of the diluents (PBS) or scramble antisense alone. Over the experimental period bi-dimensional measurements were carried out at two days interval using calipers and cross-sectional area (tumor size) were plotted (**Fig. 3a**, representative xenograft at different stages of treatments are shown in **Fig. 3b**). Experiments were repeated at least in three independent sets of experiments (using 3 replicates each time). As seen in **Figs. 3a-b**, the tumor size increased exponentially over time in the control mice that were either treated with PBS (diluents buffer) or scramble antisense. Interestingly, application of MLL1-antisense suppressed the tumor growth completely over the period of treatment in comparison to the controls (**Figs. 3a-b**). Similar to MLL1-antisense (MLL1-A3), application of MLL1-A5 antisense also effectively suppressed the growth of the xenografted tumor, though it is slightly less effective (under the similar experimental condition and doses) in comparison to MLL1-A3 (**Fig 3a**). The suppression of tumor xenograft by two independent MLL1-specific antisenses (MLL1-A3 and MLL1-A5) alleviates potential off target effects of MLL1-antisenses.

To further examine histology of MLL1-antisense treated and control tumors, we surgically removed the tumors from mice (**Fig. 4a**). Notably, the control tumors which are bigger in size (**Fig. 4a**) were tightly attached to the host mice tissue and the mice tissue invaded to the xenografted tumor tissue heavily. In contrast, MLL1-antisense treated tumors were loosely floating (did not attach to the mouse tissue) under the mice skin. After excision, the exterior

of the control tumor xenografts were found to be reddish and densely covered with network of blood vessels, whereas the number of visible blood vessels on the surface of the MLL1-antisense treated tumor xenografts were less and tumors appeared whitish (**Fig. 4a**). Dissection of tumors tissue (**Fig. 4a**, bottom panels) showed that in the control xenograft (left panel), tissue is transparent, homogenous, and healthy with some patches of highly condensed tissue (hypoxic regions). In the MLL1-antisense treated xenograft (bottom right panel **Fig. 4a**), the interior core of the tumor was semi-fluidic in nature and highly opaque indicating dead tissue. Haematoxylin and eosin (H&E) staining showed the presence of well defined cellular morphologies and nuclei in the control tumor core tissue, while there were no defined intact cells and nuclei present in the MLL1-antisense treated tumor tissue indicating dead cells (**Fig. 4b**).

To analyze the level of MLL1 expression in both control and MLL1-antisense treated xenografts, protein and RNA were isolated from the homogenized tumor tissue samples at different time of treatment (14 and 28 days) and analyzed by qPCR and western blotting. Application of MLL1-antisense specifically knocked down MLL1 (but not MLL2, control) in a temporal manner both at mRNA and protein levels (**Figs. 4c-d**). These results demonstrated that MLL1-antisense reached the xenografted tumor tissue systemically and specifically knocked down MLL1.

To investigate further, we stained the dissected tumor tissue with DAPI (that stains nucleus) and immuno-stained with MLL1 antibody and analyzed under fluorescence microscope. In the control tumor, cell nuclei were normal, round to oval shaped, and stained uniformly with DAPI, indicating healthy states of cells (**Fig. 4e**). In the MLL1-knocked down xenograft, at the core of the tumor, the cell nuclei were fragmented indicating dead cells (**Fig. 4e**). The cells were smaller, spherical, and highly dense (**Fig. 4e**). As anticipated, our immuno-staining showed higher level of MLL1 localization primarily in the cell nuclei of the control xenograft tissues (**Fig. 4e**). In the MLL1 antisense-treated tumor xenograft, MLL1 was localized in patches of fragmented nuclei and level of expression of the protein was relatively less compared to the untreated control (**Fig. 4e**). TUNEL assay demonstrated that in the control tumor, the core tissue is healthy as evidenced by well defined nuclear staining (DAPI staining, top panels, **Fig. 4f**). However, there is extensive nuclear fragmentation and DNA damage (intense dUTP labeling) in the core of the MLL1-antisense treated xenografted tumor tissue and cells were mostly dead (PI staining) (bottom panels, **Fig. 4f**). These analyses demonstrated that knockdown of MLL1 induced cell death inside xenografted tumor and resulted in disintegration of core tumor tissue resulting in suppressed tumor growth.

MLL1-knockdown suppressed the level of angiogenesis in cervical tumor xenograft

Tumor growth is critically linked with activation of different signaling pathways. Expression of growth factors and their receptors within tumor microenvironment affect both tumor growth and angiogenesis. Hypoxia in the tumor core is a critical driving force towards enhanced tumor growth and angiogenesis (47-49). Expression of angiogenic factors such as CD31 is transcriptionally regulated by vascular endothelial growth factor (VEGF), which in turn is regulated by hypoxia inducible factor- α (HIF1 α) (47). Hypoxia facilitates

stabilization of HIF1 α by inhibiting its degradation via inhibition of ubiquitination. Under hypoxic environment, HIF1 α dimerize with aryl hydrocarbon nuclear receptor translocator (ARNT) and binds to the VEGF promoter leading to its transactivation (47). VEGF binds to VEGF receptor (VEGFR) localized in the endothelial cells surface, and the activated VEGFR transactivates angiogenic factors such as CD31 that promote vasculogenesis (47-49). CD31 is well known to be expressed in the endothelial cells (located in the inner layer of blood vessels) while VEGF, basic fibroblast growth factor (bFGF), and platelet-derived growth factor (PDGF) are expressed in the basement membranes that support the differentiation and maintenance of endothelial layers in blood vessels (47-49).

As our initial observation (**Fig. 4a**) showed the presence of lesser number of blood vessels in the MLL1-antisense treated tumor in comparison to the control, we examined if knockdown of MLL1 affects the expression of HIF1 α , VEGF, and CD31 in the tumor xenograft. We isolated RNA from the control and antisense-treated tumor tissues and analyzed by qPCR. Our results demonstrated that upon application of MLL1-antisense, along with MLL1, expression of HIF1 α , VEGF, and CD31 were decreased (**Fig. 5a**). Chromatin-immunoprecipitation (ChIP with tumor tissue) analysis showed that knockdown of MLL1 resulted in decreased level of histone H3K4-trimethylation and RNA polymerase II (RNAPII) recruitment (as well as MLL1-recruitment) at the promoters of HIF1 α , VEGF, and CD31 genes (**Fig. 5b**, qPCR data in the bottom panel). Notably, histone H3K4-trimethylation is well known to be enriched in the promoter regions of transcriptionally active genes and facilitates the recruitment of RNAPII and transcription initiation. Thus, decrease in H3K4-trimethylation at the promoters of HIF1 α , VEGF, and CD31 genes, upon MLL1-depletion, suggests that MLL1-mediated histone methylation is crucial for expression of the above target genes. Together, these results demonstrated that MLL1 is a key regulator of HIF1 α , VEGF, and CD31 and hence tumor growth and angiogenesis.

Furthermore, we examined the expression of MLL1, CD31, VEGF and HIF1 α using immunofluorescence and immunohistological staining. Notably, CD31 expresses in endothelial cells of blood vessels and used as a marker for angiogenesis. Upon immunofluorescence staining with CD31, we observed that, in the control tumor, a large number of blood vessels from tumor peripheral tissue were actively invading towards the core tumor tissue (**Fig. 6a**, higher magnification/resolution images showing the localization of CD31 and MLL1 are shown in **Fig. S6**). Increased vascular branching and generation of new blood vessels were also observed in the control tumor (**Fig. 6a**, control tumor). Distinct blood vessels (CD31 staining) were also observed at the inner core of the control tumor (**Fig. 6b**, top panel). The extensive network of blood vessel formation is likely associated with high demand of oxygen supply for the rapidly growing tumor tissue. In contrast, in the MLL1-antisense treated xenograft, there was no sign (lack of CD31 staining) of blood vessel invasion or *de novo* blood vessel formation both at outer surface and at the tumor core and the tissues were mostly dead (**Fig. 6a-b**, MLL1-antisense treated). Notably, a thin layer of live xenografted human cells (as evidenced by intense layer of DAPI staining) was observed at the exterior surface of the MLL1 antisense-treated tumor (**Fig. 6a**, bottom panel, indicated by arrow). The existence of these resistant tumor cells in the external tumor surface might be supported by plenty of oxygen supply from the host tissue.

Interestingly, immunofluorescence staining showed that MLL1 and CD31 were highly localized in tissues along the line of blood vessel (**Fig. 6b**, top panels and Fig S6). A more detailed view of MLL1 and CD31 localization, surrounding a particular blood vessel (vertical cross-section) is shown in figure **6c**. Importantly, though MLL1 and CD31 are both over expressed along the vascular lining, they were not co-localized (**Fig. 6c and Fig. S6**). While CD31 was expressed in the endothelial layer (inner lining of the blood vessels), MLL1 expression was predominant in the adjacent outer layer (basement membrane) of endothelial cells (**Fig. 6b-c and Fig. S6**). To further confirm, the relative localization of MLL1 and CD31, we performed DAB staining independently (**Fig. 6d-e**). DAB staining also showed that MLL1 and CD31 were overexpressed along the line of blood vessels, CD31 is localized in the inner core (endothelial cell) of the blood vessel while MLL1 is localized at the outer layer of the blood vessel (basement membrane) (**Fig. 6d-e**). H&E staining along with CD31 and MLL1 immunostaining further confirmed that CD31 is localized in the inner core of the blood vessel while MLL1 is localized towards the outer layer of the blood vessel (Fig. 6f). Notably, the basement membrane that expresses several growth factors such as VEGF, bFGF etc, supports the differentiation and formation of endothelial layers during vascular development. Our immunofluorescence analysis also showed that VEGF is expressed in the adjacent tissue (basement membrane) expressing CD31 (endothelial cells) (**Fig. 6g**). Thus, our observations showing high expression of MLL1 in the basement membrane, and critical requirement of MLL1 in transcriptional regulation of VEGF and CD31, suggested that MLL1 plays critical roles in vasculogenesis.

HIF1 α is known to be overexpressed and enriched in the hypoxic region (50, 51). HIF1 α activates the signaling cascade that results in CD31 expression via VEGF (52, 53). Our results demonstrated that MLL1 also regulates the expression of HIF1 α , VEGF and CD31. To analyze further if MLL1 plays any roles in hypoxia signaling, we examined the expression of MLL1 and HIF1 α , in the hypoxic regions of the tumor (control xenograft). We observed that HIF1 α is overexpressed in the regions where condensed patches of opaque cell mass were distinctly visible in the control tumor, indicating the presence of hypoxic environment in those regions of tumor tissue (**Fig 7a**, top panels). Interestingly, we also observed that MLL1 is overexpressed/enriched in those hypoxic regions along with HIF1 α (**Fig 7a**, top panels). A higher resolution image showing the colocalization of MLL1 and HIF1 α in the hypoxic regions is shown in figure 7b. The overexpression of MLL1 and HIF1 α in the hypoxic region is also demonstrated by DAB staining (**Fig. 7c-d**). The overexpression/enrichment of MLL1 in the hypoxic environment and transcriptional regulation of HIF1 α by MLL1, indicated that MLL1 is associated with hypoxia signaling within tumor microenvironment. In the MLL1-antisense treated xenograft, as most tissue was dead, we did not observe any hypoxic regions as indicated by absence of MLL1 and HIF1 α staining (**Fig 7a**, bottom panels). Additionally, we observed some networks of blood vessels surrounding the hypoxic regions where MLL1 is also overexpressed (**Fig. 7a**, shown by arrow marks), indicating further the potential roles of MLL1 in *de novo* blood vessel formation driven by hypoxia.

In summary, our biochemical studies demonstrated that MLL1 plays key roles in regulation of cell cycle progression and cell viability. MLL1-knockdown affects various cell cycle

regulatory genes (including cyclin A, cyclin B and p57), resulting in cell cycle arrest in G2/M phase and apoptosis in cultured cells. Notably, MLL1 is a critical histone methylase and gene regulator, its knockdown affects expression of various genes including crucial cell cycle regulatory cyclin and p-proteins that ultimately led to cell cycle arrest and apoptosis in most cell types (both malignant and non-malignant). However, malignant cells were relatively more sensitive to MLL1-knockdown in comparison to nonmalignant cells, this may be likely because malignant cells proliferate more rapidly than normal cells, and gene expression by MLL1 is essential for cell proliferation.

Importantly, for the first time, we demonstrated that antisense-mediated MLL1-knockdown suppressed tumor growth *in vivo* (cervical cancer xenograft). MLL1-antisense reached the tumor systemically and specifically down-regulated MLL1 expression in the tumor tissue and that results in suppression of HIF1 α , VEGF and CD31 expression affecting tumor growth and level of angiogenesis. Notably, though we observed that MLL1-antisense suppressed the growth of the xenograft, it did not lead to shrinkage in tumor volume. Tissue section analysis showed that in the MLL1-antisense treated xenograft, most of the core tissue is dead (degraded). However, a layer of live cells is still present on the edge of tumor xenograft (external periphery of the tumor) that is attached to host (mice) tissue (see figure 6a, shown by arrow). These cells are more resistant to death likely because they get plenty of oxygen (and nutrients) supply from host tissue and thus are not as hypoxic as the interior core tumor tissue. The presence of this intact layer of live tumor tissue at the periphery of the tumor does not allow the shrinkage of the overall tumor volume though the interior of the existing tumor is mostly dead and degraded.

Interestingly, we found that similar to CD31, MLL1 is overexpressed along the linings of the blood vessel distinctly marking the vascular network. Though both MLL1 and CD31 are overexpressed along the vascular network, they are not co-localized. CD31 is expressed in the endothelial cells, while MLL1 is expressed in the neighboring outer layers of cells (basement membrane) that supports the formation and differentiation of endothelial layer during vasculogenesis. MLL1 is known to play critical roles in hematopoietic cell differentiation and hematopoietic stem cell is linked with origin of endothelial cells (54). Recent studies also indicate that MLL1 is critical for formation of endothelial cells (55). Our studies showing the high expression of MLL1 in the basement membrane further support its critical roles in development of endothelial cells during angiogenesis. Furthermore, overexpression of MLL1 in the hypoxic regions of the tumor where HIF1 α is overexpressed indicates a strong link between hypoxia signaling and MLL1. Overall, our studies demonstrated that MLL1 is a key player in cell proliferation, tumor growth, and knockdown of MLL1 results in suppression of tumor growth and angiogenesis *in vivo*. As MLL1 controls both cell viability and expression of angiogenic factors, the suppression of tumor growth upon MLL1-knockdown may be attributed to both inhibition of cell proliferation as well as suppression of angiogenesis. Overall, multiple of lines of evidences such as a) increased level of vascularization in the control tumor in comparison to the MLL1-antisense treated tumor, b) enrichment of MLL1 along the vascular linings, c) localization/enrichment of MLL1 in the hypoxic regions along with HIF1 α and d) crucial roles of MLL1 in transcriptional regulation of tumor growth and angiogenic factors, indicated that MLL1 is

potentially associated with vasculogenesis and its knockdown inhibits angiogenesis. Our studies demonstrated novel roles of MLLs in cell survival, tumor growth, hypoxia signaling, and angiogenesis and this opens up new avenues for novel cancer therapy.

Materials and Methods

Cell culture, transfection, RNA-protein isolation, RT-PCR and western blotting

Human cervical cancer (HeLa), human bronchialveolar carcinoma (H358), choriocarcinoma placenta (JAR), colorectal adenocarcinoma (SW-480), nonmalignant colon fibroblast (CCD-18Co), human adenocarcinoma mammary (MCF7), and nonmalignant mammary gland fibrocystic cell (MCF10) were obtained from American type cell culture collection (ATCC), grown and maintained as described previously (41, 42). For transfection, cells were grown up to 60% confluency in 60 mm culture plate and then transfected with MLL1-antisense oligonucleotides (Table S1) using ifect (Molecula) transfection reagent (41, 42). RNA was isolated and quantified from antisense-treated and control cells, reverse transcribed to cDNA and subjected to real-time PCR (qPCR) as described previously (details in supplementary information). Proteins from the antisense-treated and control cells were analyzed by western blotting using antibodies against MLL1 (Abgent), MLL2, (Abgent) and β -actin (Sigma).

Analyzing cell viability, morphology and cytotoxicity

The cytotoxicity of MLL1-antisenses were determined by MTT assay as described previously (56). For analyzing effect of MLL1 antisense on cell viability and cell morphology, HeLa cells were grown in 60 mm culture plates and transfected with MLL1 (or scramble) antisense for 48 h, stained with trypan blue (10 min) and visualized under differential interference contrast (DIC) setting of a microscope (Nikon Eclipse TE2000-U, Japan).

Flow-cytometry analysis, TUNEL assay, Caspase-3/7 activity assay

HeLa cells were transfected with MLL1 and scramble antisense oligonucleotides separately for 48 h, harvested, fixed in 70% ethanol for 2 h, washed twice with PBS and stained with propidium iodide (final concentration, 0.5 μ g/mL). The cells were analyzed by flow cytometry, using a Beckman Coulter (Fullerton, CA, USA) Cytomics FC500 flow cytometry analyzer as described previously (21). TUNEL and Caspase assays were performed as described by us previously (also see the supplementary information) (56).

Chromatin immuno-precipitation (ChIP) assay

Cells were transfected with MLL1 and scramble antisense for 48 h. For ChIP assay, cells were fixed with 1 % formaldehyde, washed, resuspended in lysis buffer (1 % SDS, 10 mM EDTA, 50 mM Tris/HCl, pH 8, 1X protease inhibitors and 0.2 mM PMSF), sonicated until chromatin was sheared to an average DNA fragment length of 0.2 - 0.5 kb and subjected to ChIP assay (as described previously using different antibodies as needed (21, 41, 42).

Animal toxicity and cervical cancer xenografts

All animal experiments were carried out using the IACUC approved protocol and every care and precautions were taken to minimize the pain/stress on the animal. Animals were hosted in the institutional (UTA) animal care facility under the supervision of trained personal. Prior to getting into the xenograft experiments, the animal toxicity of each of the antisense oligonucleotides were examined using nude mouse. Six weeks old athymic nude (nu/nu) mice (obtained from Harlan, Indianapolis, IN) were used for these experiments. For the toxicity analysis, we injected intraperitoneally three different doses (100, 300 and 500 $\mu\text{g}/20$ gm body weight) of MLL1 and scramble antisense into six week old nude mouse (3 replicates each) and then monitored the health of each mouse on a daily basis for a month. We monitored the body weight at every 4 days intervals after treatment with antisense.

For the xenograft experiments, 2×10^6 human cervical cancer cells (HeLa cell in 100 μl of PBS) were injected subcutaneously (near the right back limb) (57, 58). Animals were examined daily for signs of tumor growth and behavior. Once the tumor size reached ~ 32 mm² (2 to 3 weeks after injection of cells) we administered MLL1-antisense intraperitoneally (PBS solution, twice in a week, 300 $\mu\text{g}/20$ gm body weight, in three parallel replicates, continued for a month). Experiments were repeated at least three times. Control mice were injected with equal volume of the diluents (PBS) or scramble antisense alone. Tumor sizes were measured every two days intervals and bi-dimensional measurements were carried out using calipers and tumor cross-sectional area (tumor size) were plotted. The normal growth habit of the animals was observed and body weight of the animals was recorded over the experimental period.

Immuno-histological staining and RNA and protein analysis in tumor tissue

For RNA and protein analysis, tumors were directly excised from euthanized mice, flash frozen in liquid nitrogen, homogenized and subjected to RNA (ZyGEM kit) and protein extraction that were then subjected to qPCR and western blotting.

For immuno-histochemical staining, mice were sequentially perfused with cold PBS (pH 7.4), followed by 4% paraformaldehyde (in PBS), and then xenografted tumors were removed, cryoprotected in PBS containing 30% sucrose and sectioned. Immuno-histochemical staining (fluorescent) of the xenografted tumor sections was done as described by previously (21, 59). In brief, sections were blocked by incubating in presence of goat serum, incubated (2 h) with the respective primary antibodies (CD31, MLL1, HIF α), washed and incubated with FITC or rhodamine conjugated secondary antibodies (Jackson Immuno Research Laboratories). Nuclear counterstaining was performed with DAPI. Immuno-stained cells were mounted and observed under a fluorescence microscope. For DAB staining and immuno-histological analysis, the cryoprotected xenografted tumor sections were incubated in blocking buffer (containing donkey serum) and then with primary antibodies specific to MLL1, CD31, HIF α and VEGF. Sections were then incubated with biotinylated donkey secondary antibody followed by avidin–biotin complexes (ABC), followed by peroxidase labeling using a DAB substrate kit (Vector Laboratories). Sections were mounted with DPX mounting solution and examined under light microscope.

Chromatin immuno-precipitation (ChIP) assay with tumor tissue

For chromatin immuno-precipitation (ChIP) mice were sequentially perfused with cold PBS (pH 7.4), followed by 4% paraformaldehyde (in PBS), and then xenografted tumors were removed, cryoprotected in PBS containing 30% sucrose and sectioned. The tissue was homogenized and sonicated in presence of cell lysis buffer to shear the chromatin to a fragment length of ~ 0.2 - 0.5 kb. The fragmented chromatin was pre-cleaned and then incubated with MLL1, RNAPII (Abcam), H3K4-tri-methyl (Upstate) and β -actin antibodies overnight, subjected to immunoprecipitation using agarose beads. The immunoprecipitated chromatin was deproteinized and PCR-amplified using promoter specific primers (qPCR).

Supplementary Material

Refer to Web version on PubMed Central for supplementary material.

Acknowledgements

We thank Linda Perrotti and Samara Morris-Bobzean for technical assistance with tissue sectioning and Mandal lab members for discussion. Mandal research is supported by grants from NIH (1R15 ES019129-01, 2R15 CA113747-02) and NSF (0821969).

References

1. Corey DR. Telomerase inhibition, oligonucleotides, and clinical trials. *Oncogene*. Jan 21; 2002 21(4):631–7. [PubMed: 11850789]
2. Gleave ME, Monia BP. Antisense therapy for cancer. *Nat Rev Cancer*. Jun; 2005 5(6):468–79. [PubMed: 15905854]
3. Lu B, Mu Y, Cao C, Zeng F, Schneider S, Tan J, et al. Survivin as a therapeutic target for radiation sensitization in lung cancer. *Cancer Res*. Apr 15; 2004 64(8):2840–5. [PubMed: 15087401]
4. Ryan BM, O'Donovan N, Duffy MJ. Survivin: a new target for anti-cancer therapy. *Cancer Treat Rev*. Nov; 2009 35(7):553–62. [PubMed: 19559538]
5. Halatsch ME, Schmidt U, Behnke-Mursch J, Unterberg A, Wirtz CR. Epidermal growth factor receptor inhibition for the treatment of glioblastoma multiforme and other malignant brain tumours. *Cancer Treat Rev*. Apr; 2006 32(2):74–89. [PubMed: 16488082]
6. Kang CS, Zhang ZY, Jia ZF, Wang GX, Qiu MZ, Zhou HX, et al. Suppression of EGFR expression by antisense or small interference RNA inhibits U251 glioma cell growth in vitro and in vivo. *Cancer Gene Ther*. May; 2006 13(5):530–8. [PubMed: 16410821]
7. Kurdistan SK. Histone modifications in cancer biology and prognosis. *Prog Drug Res*. 2011; 67:91–106. [PubMed: 21141726]
8. Goldberg AD, Allis CD, Bernstein E. Epigenetics: a landscape takes shape. *Cell*. Feb 23; 2007 128(4):635–8. [PubMed: 17320500]
9. Sims RJ 3rd, Reinberg D. From chromatin to cancer: a new histone lysine methyltransferase enters the mix. *Nat Cell Biol*. Aug; 2004 6(8):685–7. [PubMed: 15303093]
10. Travers J, Blagg J, Workman P. Epigenetics: Targeting leukemia on the DOT. *Nat Chem Biol*. Oct; 7(10):663–5. [PubMed: 21873997]
11. Dawson MA, Prinjha RK, Dittman A, Giotopoulos G, Bantscheff M, Chan WI, et al. Inhibition of BET recruitment to chromatin as an effective treatment for MLL-fusion leukaemia. *Nature*. Oct 2.2011
12. Ansari KI, Mishra BP, Mandal SS. Human CpG binding protein interacts with MLL1, MLL2 and hSet1 and regulates Hox gene expression. *Biochim Biophys Acta*. Jan; 2008 1779(1):66–73. [PubMed: 18082152]

13. Canaani E, Nakamura T, Rozovskaia T, Smith ST, Mori T, Croce CM, et al. ALL-1/MLL1, a homologue of *Drosophila* TRITHORAX, modifies chromatin and is directly involved in infant acute leukaemia. *Br J Cancer*. Feb 23; 2004 90(4):756–60. [PubMed: 14970849]
14. Dou YL, Milne TA, Tackett AJ, Smith ER, Fukuda A, Wysocka J, et al. Physical association and coordinate function of the H3K4 methyltransferase MLL1 and the H4K16 acetyltransferase MOF. *Cell*. Jun; 2005 121(6):873–85. [PubMed: 15960975]
15. Glaser S, Schaft J, Lubitz S, Vintersten K, van der Hoeven F, Tufteland KR, et al. Multiple epigenetic maintenance factors implicated by the loss of Mll2 in mouse development. *Development*. Apr; 2006 133(8):1423–32. [PubMed: 16540515]
16. Guenther MG, Jenner RG, Chevalier B, Nakamura T, Croce CM, Canaani E, et al. Global and Hox-specific roles for the MLL1 methyltransferase. *Proc Natl Acad Sci U S A*. Jun 14; 2005 102(24):8603–8. [PubMed: 15941828]
17. Hanson RD, Hess JL, Yu BD, Ernst P, van Lohuizen M, Berns A, et al. Mammalian Trithorax and polycomb-group homologues are antagonistic regulators of homeotic development. *Proc Natl Acad Sci U S A*. Dec 7; 1999 96(25):14372–7. [PubMed: 10588712]
18. Hess JL. MLL: a histone methyltransferase disrupted in leukemia. *Trends Mol Med*. Oct; 2004 10(10):500–7. [PubMed: 15464450]
19. Lee J, Saha PK, Yang QH, Lee S, Park JY, Suh Y, et al. Targeted inactivation of MLL3 histone H3-Lys-4 methyltransferase activity in the mouse reveals vital roles for MLL3 in adipogenesis. *Proc Natl Acad Sci U S A*. Dec 9; 2008 105(49):19229–34. [PubMed: 19047629]
20. Lee JH, Skalnik DG. CpG-binding protein is a nuclear matrix- and euchromatin-associated protein localized to nuclear speckles containing human trithorax. Identification of nuclear matrix targeting signals. *J Biol Chem*. Nov 1; 2002 277(44):42259–67. [PubMed: 12200428]
21. Mishra BP, Ansari KI, Mandal SS. Dynamic association of MLL1, H3K4 trimethylation with chromatin and Hox gene expression during the cell cycle. *FEBS J*. Mar; 2009 276(6):1629–40. [PubMed: 19220463]
22. Ruthenburg AJ, Wang WK, Graybosch DM, Li HT, Allis CD, Patel DJ, et al. Histone H3 recognition and presentation by the WDR5 module of the MLL1 complex. *Nature Structural & Molecular Biology*. Aug; 2006 13(8):704–12.
23. Yokoyama A, Wang Z, Wysocka J, Sanyal M, Aufiero DJ, Kitabayashi I, et al. Leukemia proto-oncoprotein MLL forms a SET1-like histone methyltransferase complex with menin to regulate Hox gene expression. *Mol Cell Biol*. Jul; 2004 24(13):5639–49. [PubMed: 15199122]
24. Bhaumik SR, Smith E, Shilatifard A. Covalent modifications of histones during development and disease pathogenesis. *Nat Struct Mol Biol*. Nov; 2007 14(11):1008–16. [PubMed: 17984963]
25. Cuthbert G, Thompson K, McCullough S, Watmore A, Dickinson H, Telford N, et al. MLL amplification in acute leukaemia: a United Kingdom Cancer Cytogenetics Group (UKCCG) study. *Leukemia*. Nov; 2000 14(11):1885–91. [PubMed: 11069023]
26. Ansari KI, Mandal SS. Mixed lineage leukemia: roles in gene expression, hormone signaling and mRNA processing. *FEBS J*. Mar 4. 2010 277:1790–804. [PubMed: 20236313]
27. Parsons DW, Li M, Zhang X, Jones S, Leary RJ, Lin JC, et al. The genetic landscape of the childhood cancer medulloblastoma. *Science*. Jan 28; 2011 331(6016):435–9. [PubMed: 21163964]
28. Pasqualucci L, Trifonov V, Fabbri G, Ma J, Rossi D, Chiarenza A, et al. Analysis of the coding genome of diffuse large B-cell lymphoma. *Nat Genet*. Sep; 2011 43(9):830–7. [PubMed: 21804550]
29. Paulussen AD, Stegmann AP, Blok MJ, Tserpelis D, Posma-Velter C, Detisch Y, et al. MLL2 mutation spectrum in 45 patients with Kabuki syndrome. *Hum Mutat*. Feb; 2010 32(2):E2018–25. [PubMed: 21280141]
30. Saigo K, Yoshida K, Ikeda R, Sakamoto Y, Murakami Y, Urashima T, et al. Integration of hepatitis B virus DNA into the myeloid/lymphoid or mixed-lineage leukemia (MLL4) gene and rearrangements of MLL4 in human hepatocellular carcinoma. *Hum Mutat*. May; 2008 29(5):703–8. [PubMed: 18320596]
31. Fujimoto A, Totoki Y, Abe T, Boroevich KA, Hosoda F, Nguyen HH, et al. Whole-genome sequencing of liver cancers identifies etiological influences on mutation patterns and recurrent mutations in chromatin regulators. *Nat Genet*. May 27.

32. Wang XX, Fu L, Li X, Wu X, Zhu Z, Fu L, et al. Somatic mutations of the mixed-lineage leukemia 3 (MLL3) gene in primary breast cancers. *Pathol Oncol Res.* Jun; 17(2):429–33. [PubMed: 21116761]
33. Watanabe Y, Castoro RJ, Kim HS, North B, Oikawa R, Hiraishi T, et al. Frequent alteration of MLL3 frameshift mutations in microsatellite deficient colorectal cancer. *PLoS One.* 6(8):e23320. [PubMed: 21853109]
34. Crawford BD, Hess JL. MLL core components give the green light to histone methylation. *ACS Chem Biol.* Sep 19; 2006 1(8):495–8. [PubMed: 17168535]
35. Dou Y, Milne TA, Ruthenburg AJ, Lee S, Lee JW, Verdine GL, et al. Regulation of MLL1 H3K4 methyltransferase activity by its core components. *Nat Struct Mol Biol.* Aug; 2006 13(8):713–9. [PubMed: 16878130]
36. Deng LW, Chiu I, Strominger JL. MLL 5 protein forms intranuclear foci, and overexpression inhibits cell cycle progression. *Proc Natl Acad Sci U S A.* Jan 20; 2004 101(3):757–62. [PubMed: 14718661]
37. Hsieh JJD, Ernst P, Erdjument-Bromage H, Tempst P, Korsmeyer SJ. Proteolytic cleavage of MLL generates a complex of N- and C-terminal fragments that confers protein stability and subnuclear localization. *Molecular and Cellular Biology.* Jan; 2003 23(1):186–94. [PubMed: 12482972]
38. Ansari KI, Hussain I, Das HK, Mandal SS. Overexpression of human histone methylase MLL1 upon exposure to a food contaminant mycotoxin, deoxynivalenol. *Febs J.* May 4.2009 276:3299–307. [PubMed: 19438726]
39. Liu H, Takeda S, Kumar R, Westergard TD, Brown EJ, Pandita TK, et al. Phosphorylation of MLL by ATR is required for execution of mammalian S-phase checkpoint. *Nature.* Sep 16; 467(7313): 343–6. [PubMed: 20818375]
40. Lee JS, Kim KI, Baek SH. Nuclear receptors and coregulators in inflammation and cancer. *Cancer Lett.* Aug 28; 2008 267(2):189–96. [PubMed: 18433989]
41. Ansari KI, Hussain I, Shrestha B, Kasiri S, Mandal SS. HOXC6 Is transcriptionally regulated via coordination of MLL histone methylase and estrogen receptor in an estrogen environment. *J Mol Biol.* Aug 12; 2011 411(2):334–49. [PubMed: 21683083]
42. Ansari KI, Shrestha B, Hussain I, Kasiri S, Mandal SS. Histone Methylases MLL1 and MLL3 Coordinate with Estrogen Receptors in Estrogen-Mediated HOXB9 Expression. *Biochemistry.* May 3; 2011 50(17):3517–27. [PubMed: 21428455]
43. Bromleigh VC, Freedman LP. p21 is a transcriptional target of HOXA10 in differentiating myelomonocytic cells. *Genes Dev.* Oct 15; 2000 14(20):2581–6. [PubMed: 11040212]
44. Obaya AJ, Sedivy JM. Regulation of cyclin-Cdk activity in mammalian cells. *Cell Mol Life Sci.* Jan; 2002 59(1):126–42. [PubMed: 11846025]
45. Satyanarayana A, Kaldis P. Mammalian cell-cycle regulation: several Cdks, numerous cyclins and diverse compensatory mechanisms. *Oncogene.* Aug 20; 2009 28(33):2925–39. [PubMed: 19561645]
46. Joaquin M, Gubern A, Gonzalez-Nunez D, Josue Ruiz E, Ferreiro I, de Nadal E, et al. The p57 CDKi integrates stress signals into cell-cycle progression to promote cell survival upon stress. *Embo J.* May 8.2012
47. Lendahl U, Lee KL, Yang H, Poellinger L. Generating specificity and diversity in the transcriptional response to hypoxia. *Nat Rev Genet.* Dec; 2009 10(12):821–32. [PubMed: 19884889]
48. Ricci-Vitiani L, Pallini R, Biffoni M, Todaro M, Invernici G, Cenci T, et al. Tumour vascularization via endothelial differentiation of glioblastoma stem-like cells. *Nature.* Dec 9; 2010 468(7325):824–8. [PubMed: 21102434]
49. Wang R, Chadalavada K, Wilshire J, Kowalik U, Hovinga KE, Geber A, et al. Glioblastoma stem-like cells give rise to tumour endothelium. *Nature.* Dec 9; 468(7325):829–33. [PubMed: 21102433]
50. Monti E, Gariboldi MB. HIF-1 as a target for cancer chemotherapy, chemosensitization and chemoprevention. *Curr Mol Pharmacol.* Jan; 4(1):62–77. [PubMed: 20958262]
51. Lee KA, Roth RA, LaPres JJ. Hypoxia, drug therapy and toxicity. *Pharmacol Ther.* Feb; 2007 113(2):229–46. [PubMed: 17046066]

52. Li Z, Bao S, Wu Q, Wang H, Eyler C, Sathornsumetee S, et al. Hypoxia-inducible factors regulate tumorigenic capacity of glioma stem cells. *Cancer Cell*. Jun 2; 2009 15(6):501–13. [PubMed: 19477429]
53. Hendriksen EM, Span PN, Schuurung J, Peters JP, Sweep FC, van der Kogel AJ, et al. Angiogenesis, hypoxia and VEGF expression during tumour growth in a human xenograft tumour model. *Microvasc Res*. Mar; 2009 77(2):96–103. [PubMed: 19118564]
54. Hess JL, Yu BD, Li B, Hanson R, Korsmeyer SJ. Defects in yolk sac hematopoiesis in Mll-null embryos. *Blood*. Sep 1; 1997 90(5):1799–806. [PubMed: 9292512]
55. Diehl F, Rossig L, Zeiher AM, Dimmeler S, Urbich C. The histone methyltransferase MLL is an upstream regulator of endothelial-cell sprout formation. *Blood*. Feb 15; 2007 109(4):1472–8. [PubMed: 17047146]
56. Ansari KI, Grant JD, Kasiri S, Woldemariam G, Shrestha B, Mandal SS. Manganese(III)-salens induce tumor selective apoptosis in human cells. *J Inorg Biochem*. Feb 24.2009 103:818–26. [PubMed: 19297027]
57. Singhal SS, Singhal J, Yadav S, Dwivedi S, Boor PJ, Awasthi YC, et al. Regression of lung and colon cancer xenografts by depleting or inhibiting RLIP76 (Ral-binding protein 1). *Cancer Res*. May 1; 2007 67(9):4382–9. [PubMed: 17483352]
58. Wang H, Hang J, Shi Z, Li M, Yu D, Kandimalla ER, et al. Antisense oligonucleotide targeted to RIalpha subunit of cAMP-dependent protein kinase (GEM231) enhances therapeutic effectiveness of cancer chemotherapeutic agent irinotecan in nude mice bearing human cancer xenografts: in vivo synergistic activity, pharmacokinetics and host toxicity. *Int J Oncol*. Jul; 2002 21(1):73–80. [PubMed: 12063552]
59. Wang D, Stockard CR, Harkins L, Lott P, Salih C, Yuan K, et al. Immunohistochemistry in the evaluation of neovascularization in tumor xenografts. *Biotech Histochem*. Jun; 2008 83(3):179–89. [PubMed: 18846440]

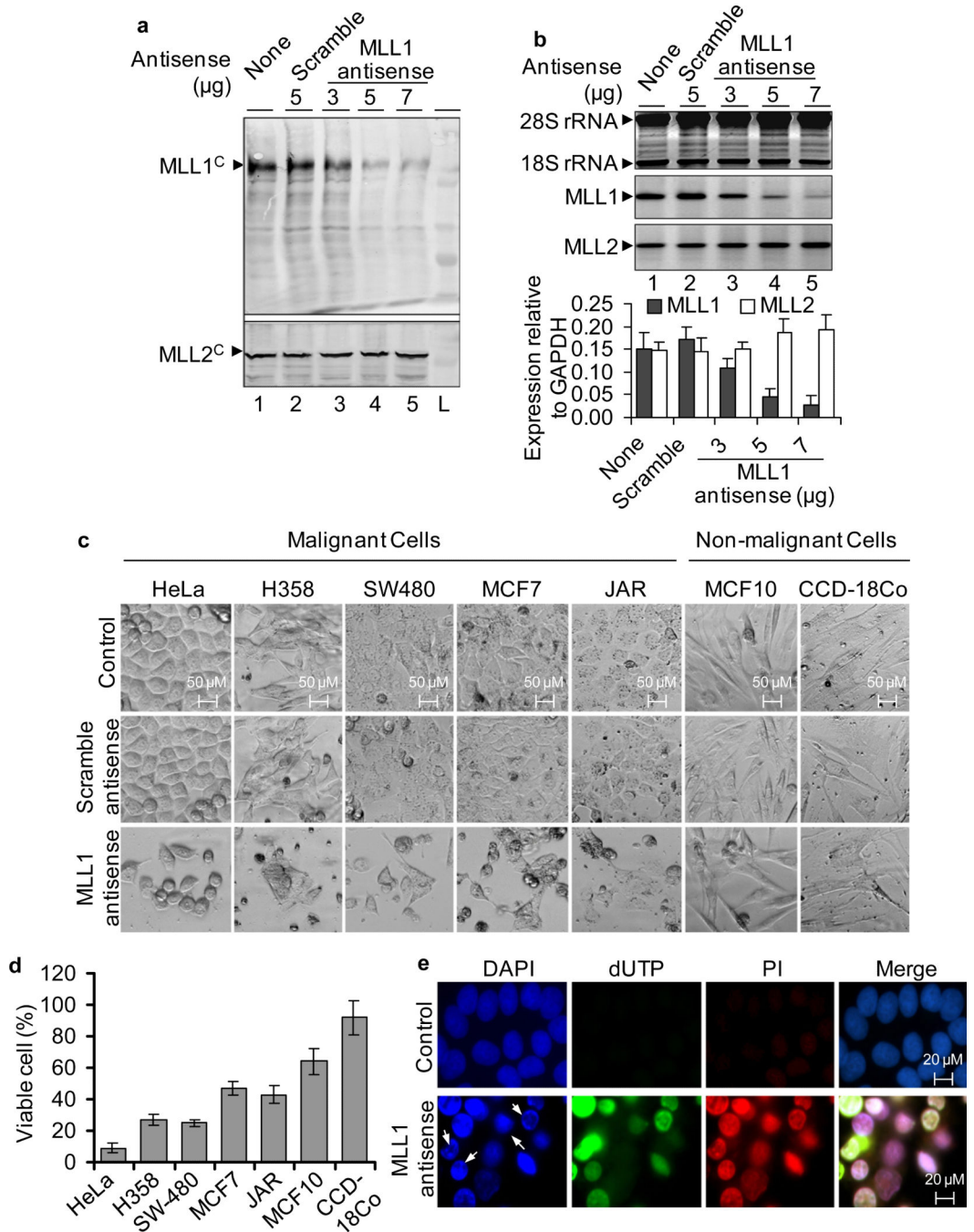


Figure 1. Effect of MLL1-knockdown on cell viability

(a-b) Knockdown of MLL1: HeLa cells were transfected with varying concentrations of MLL1-antisense or scramble antisense for 48 h. (a) Proteins from control and antisense-treated cells were analyzed by western blotting using MLL1 and MLL2 (control) antibodies. Lane 1: control cells; lane 2: cells transfected with scramble antisense; lanes 3-5: cells transfected with 3-7 µg of MLL1 antisense. (b) RNA from control and antisense-treated cells were reverse transcribed and analyzed by regular PCR (top panel) and qPCR (bottom panel) using primers specific to MLL1, MLL2 (control) and β-actin (control). Each reaction

in qPCR was done in three parallel replicates and experiment was repeated at least twice ($n = 6$, $p < 0.05$) (c) Microscopic analysis of MLL1-antisense treated cells. Different types of cancer and normal cells [HeLa (cervical cancer), H358 (lung cancer), SW-480 (colon cancer), JAR (placenta cancer), CCD-18Co (colon normal), MCF7 (breast cancer), and MCF10 (breast normal)] were transfected with 7 μg MLL1-specific or scramble antisense for 48 h and then cells were visualized under a microscope. (d) Quantification of viable cells using MTT assay: Different types of cancer and non-cancer cells were transfected with 7 μg MLL1-antisense or scramble antisense for 48 h and then subjected to MTT assay. The relative (%) cell viability (MLL1-antisense vs scramble) was plotted for different cell lines. Bars indicated standard error ($n = 10$, $p < 0.05$) (e) TUNEL assay: HeLa cells were transfected with MLL1 antisense for 48 h, fixed in 70 % EtOH and subjected to terminal nicked end-labeling using fluorescent dUTP. In parallel cells were also stained with DAPI (nuclear staining, blue fluorescence) and propidium iodide (PI that stains nucleus of dead cells, red color). dUTP stained green speckles represent apoptotic cells with fragmented nuclei.

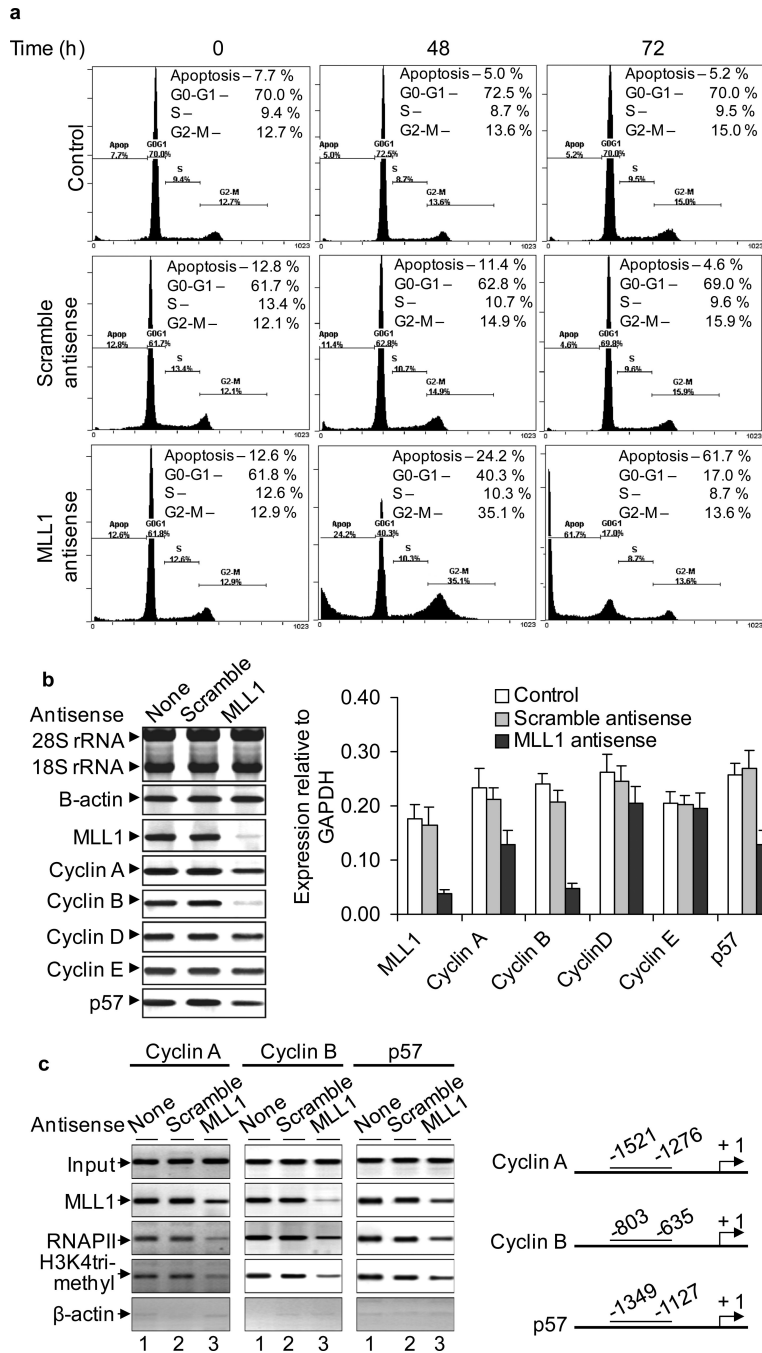


Figure 2. Roles of MLL1 in cell cycle progression

(a) FACS analysis: HeLa cells were transfected with MLL1- or scramble antisense for different time periods (24-72 hr), fixed in 70 % ethanol, and analyzed by flow cytometer. Percent (%) cell populations at different stages of cell cycles are listed within the panels. (b) Effect of MLL1 knockdown on regulation of cyclins and p-proteins. HeLa cells were transfected with MLL1-antisense and scramble antisense for 48 h. Cells were harvested and RNA extracts were subjected to RT-PCR analysis by using primer specific to cycle regulatory genes cyclin A, cyclin B, cyclin D, cyclin E, p57. 28S and 18S rRNA was used as

loading control. Real time quantification relative to GAPDH is shown in the right panel. Bars indicate standard errors ($n = 3$, $p < 0.05$). (c) ChIP analysis. MLL1-antisense and scramble antisense treated cells were fixed in formaldehyde, sonicated to shear the chromatin and then subjected to immuno-precipitated by using MLL1, H3K4 tri-methyl and RNAPII specific antibodies. β -actin specific antibody was used as non-specific control. The immuno-precipitated chromatin was PCR-amplified with primer specific to promoter regions of cyclin A, cyclin B, and p57. The position of the amplicons are shown the right panels.

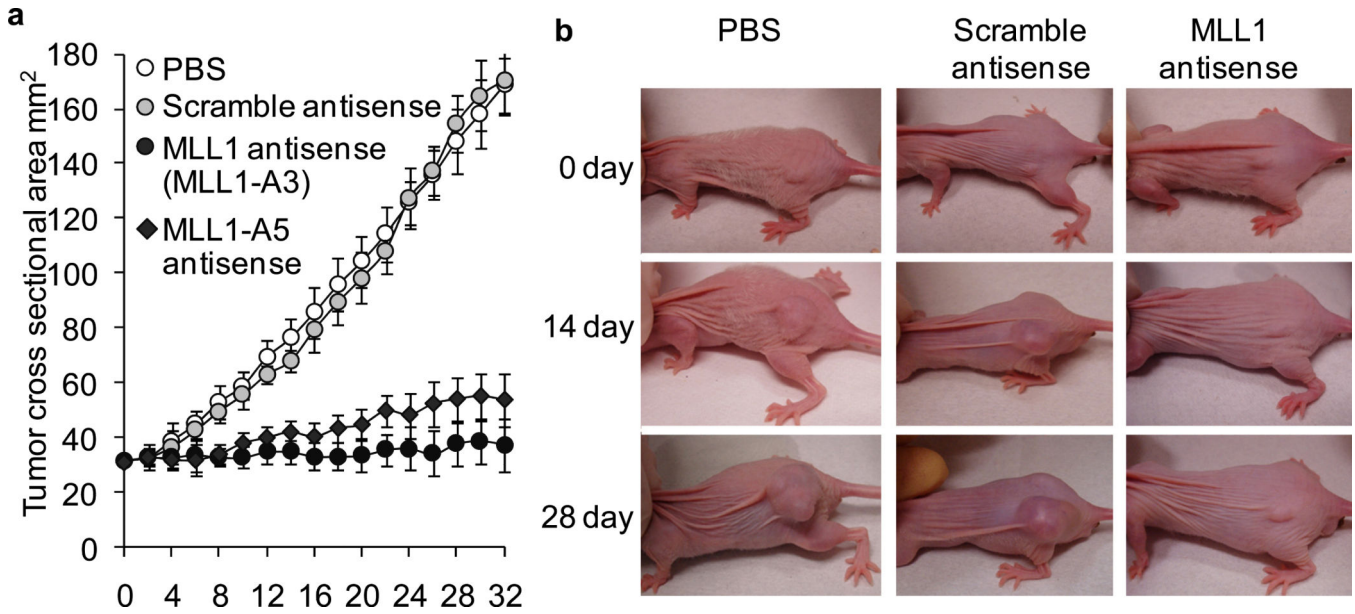


Figure 3. Regression of cervical cancer xenograft by MLL1-antisense

HeLa cells were subcutaneously injected on the right hinge region of six weeks old athymic nude (nu/nu) mice. Mice were regularly observed for appearance of tumor. Once the tumor reached about 32 mm² of cross-sectional area, mice were intraperitoneally administered with MLL1-antisense (MLL1-A3 and MLL1-A5, 300 µg/ 20 gm body weight) on the left hinge region at 4 days interval for 4 weeks. Control mice were administered with either PBS (diluent) or a same doze of scramble antisense. Tumor sizes were measured using a slid caliper at every two days intervals. **(a)** Area of tumor cross-sections was plotted against time. Bars indicated standard errors (n = 9, p < 0.05). **(b)** Representative pictures of the control and treated (MLL1-A3) mice at different stages of antisense treatments are shown.

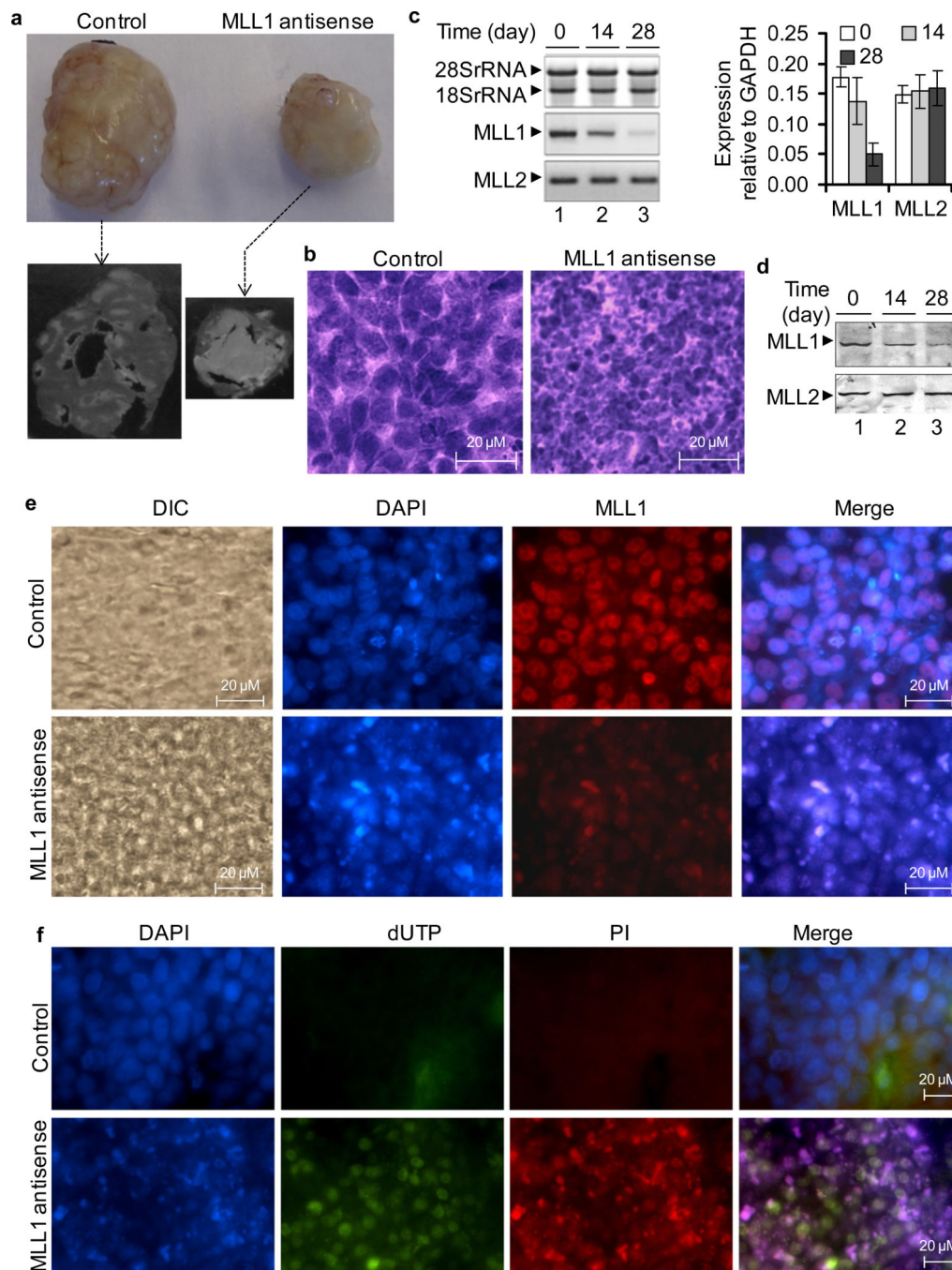


Figure 4. Antisense-mediated MLL1 knockdown, analysis of target gene expression and tumor histology

(a) Representative image of the control and MLL1-antisense treated tumor xenograft (excised after 28 days of treatment) is shown in the top panel. Cross-sections of above respective tumors are shown at bottom panel. (b) Haematoxylin/eosin (H&E) staining of the tumor cross sections of control and MLL1-antisense treated tumors. (c) RT-PCR analysis: RNA was isolated from control and MLL1-antisense treated tumor tissues and subjected to RT-PCR analysis using MLL1 and MLL2 (as control) specific primers. The rRNA (28S and

18S) was shown as loading control. The real-time quantification of MLL1 expression relative to GAPDH is shown in right panel. Bars indicate standard error ($n = 3$, $p < 0.05$). **(d)** Western blotting: Proteins from the control and MLL1-antisense treated tumors were analyzed by western blotting using antibodies specific to MLL1 and MLL2 (control). **(e)** Immunofluorescence staining: The control and MLL1-antisense treated mice with cervical cancer xenograft were perfused with 4% paraformaldehyde at 28th day of treatment. The tumors were excised, sectioned and subjected to immunofluorescence staining with MLL1 antibody. Nuclear counter-staining was done with DAPI and analyzed under fluorescence microscope. Representative images showing the cellular morphology (DIC), nuclear integrity (DAPI) and MLL1 expression in the control and MLL1-antisense treated tumors are shown. **(f)** TUNEL assay: Paraformaldehyde perfused tumor sections were subjected to terminal nicked end-labeling using fluorescent dUTP. In parallel the sections were also stained with DAPI and propidium iodide. dUTP stained green speckles represent apoptotic cells with fragmented nuclei.

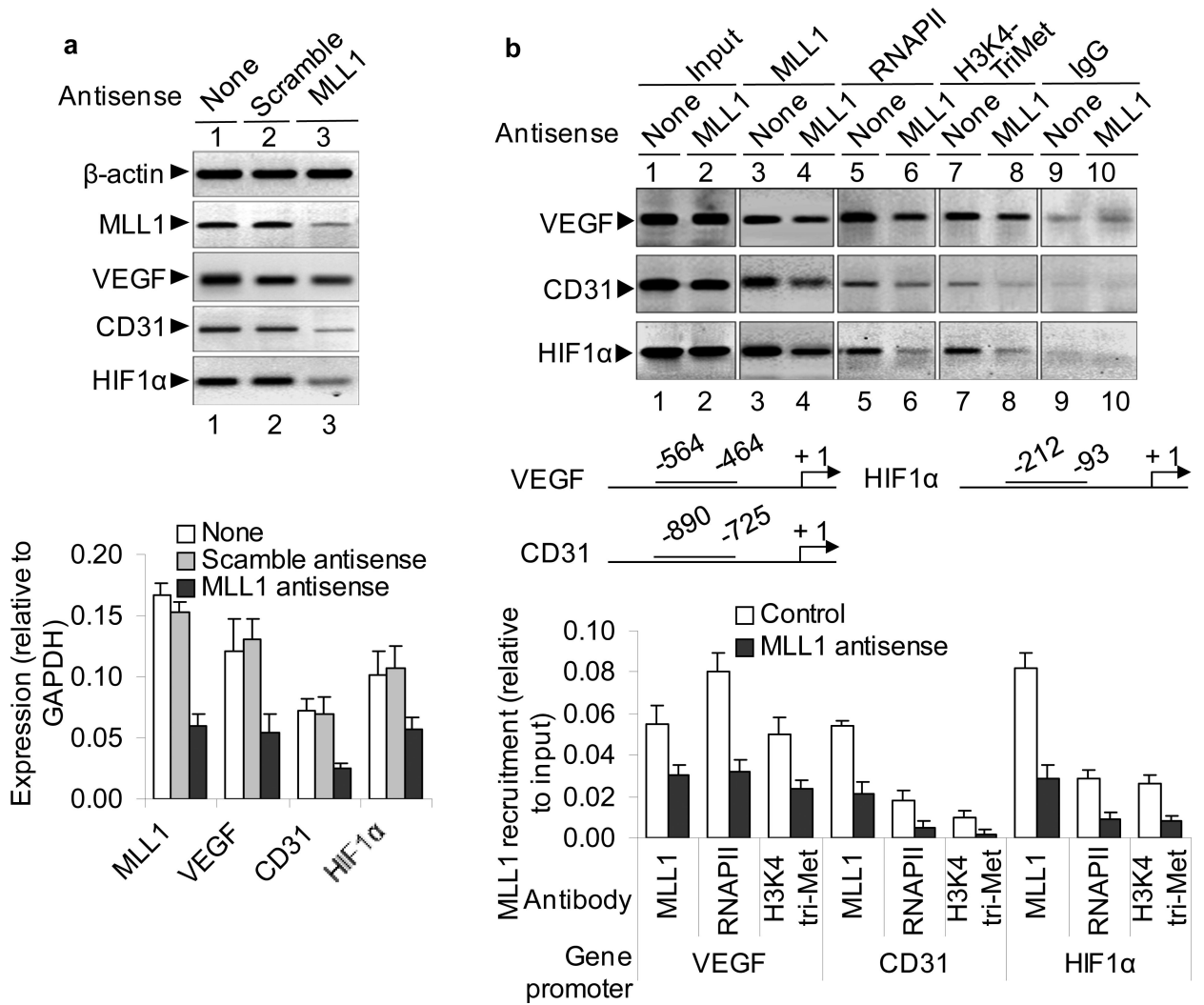


Figure 5. Effect of MLL1-knockdown on expression of tumor growth, angiogenic, and hypoxia signaling factors

(a) Analysis of growth and angiogenic factors by qPCR: RNA from the control and MLL1-antisense treated tumor tissues were reverse transcribed and analyzed by RT-PCR using primers specific to MLL1, VEGF, CD31, HIF1α and β-actin (control). The real-time quantifications of each gene expression (relative to GAPDH) are shown in bottom panel. Bars indicate standard error (n = 3, p < 0.05). (b) ChIP assay showing the binding of MLL1, RNAPII and level of H3K4-trimethylation in the promoters of VEGF, CD31 and HIF1α upon MLL1 depletion. The control and MLL1-antisense treated mice with cervical cancer xenograft were perfused with 4 % formaldehyde at 28th day of treatment. The tumors were excised, homogenized, sonicated to shear the chromatin, and subjected to ChIP assay using antibodies specific to MLL1, RNAP II, and H3K4-trimethyl antibodies. The immunoprecipitated DNA was PCR-amplified using primer specific to promoter region of VEGF, CD31 and HIF1α. IgG was used as antibody control. Real-time quantification of MLL1 and RNAPII recruitment and level of H3K4 trimethylation relative to input is shown in the bottom panel. Bars indicate standard error (n = 3, p < 0.05). The position of the amplicons are shown the middle panels.

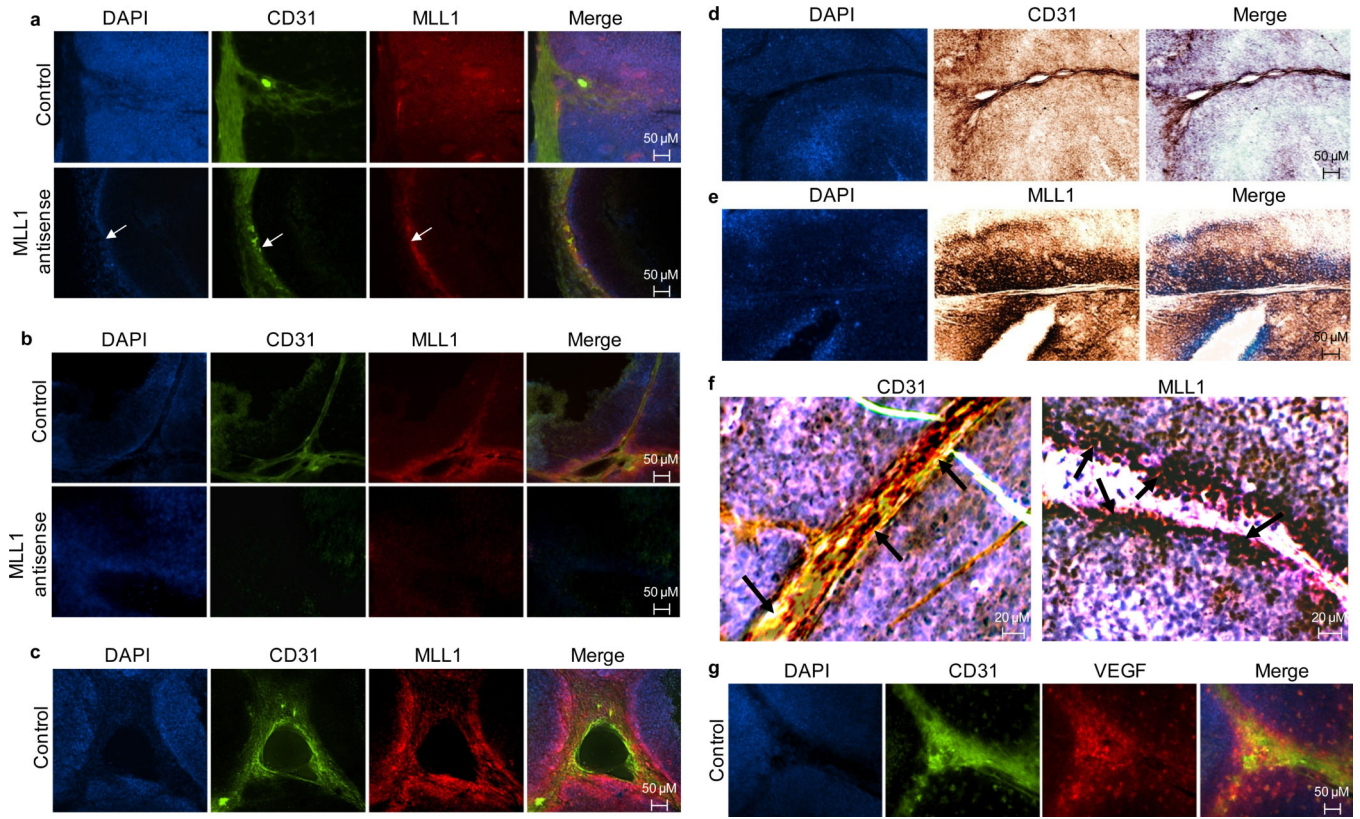


Figure 6. Roles MLL1 in vasculogenesis

(a-c) Co-immunofluorescence staining of CD31 and MLL1. Para-formaldehyde perfused tumor xenograft tissue (control and MLL1-antisense treated) were sectioned and subjected to co-immunostaining with CD31 and MLL1 antibodies, followed by staining with FITC and rhodamine conjugated secondary antibodies. Nuclear counter staining was done with DAPI and then visualized under fluorescence microscope. Representative images of the exterior periphery (a) and interior core (b) of the control and MLL1-antisense treated xenografted tumor tissue are shown. Arrows indicate live human tissue at the exterior periphery of MLL1-antisense treated xenograft. (c) Immunofluorescence staining showing localization of MLL1 and CD31 in surroundings of a vascular channel (vertical cross-section). (d-e) DAB staining showing the localization of MLL1 and CD31 around vascular track. The cervical xenograft containing mice were perfused with 4% formaldehyde and the tumors were excised, sectioned and subjected to DAB staining using MLL1 and CD31 antibodies, independently. Nuclear counter staining was done with DAPI. (f) H&E staining of tumor cross section along with DAB staining of CD31 and MLL1. Positions of CD31 and MLL1 along the vascular linings are shown by arrows. (g) Immunofluorescence staining of CD31 and VEGF in the control tumor tissue.

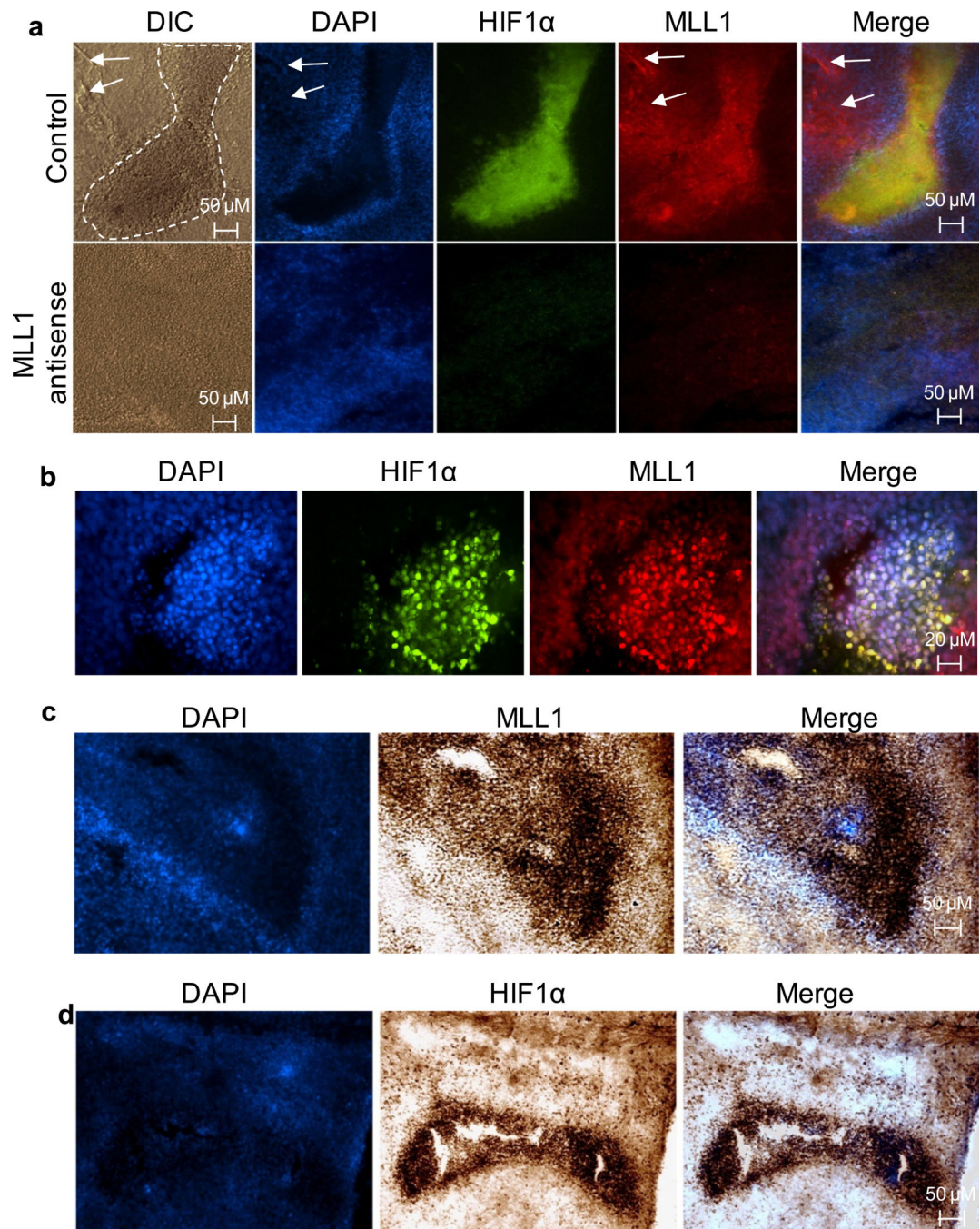


Figure 7. Histochemical analysis showing the localization of HIF1 α and MLL1 around hypoxic regions

(a-b) Co-immunofluorescence staining of HIF1 α and MLL1: Para-formaldehyde perfused tumor xenograft tissue (control and MLL1-antisense treated) were sectioned and subjected to co-immunostaining with HIF1 α and MLL1 antibodies, followed by staining with FITC and rhodamine conjugated secondary antibodies. Nuclear counter staining was done with DAPI and then visualized under fluorescence microscope. In the control tumor, hypoxic regions are distinctly visible (marked with dashed boundary in DIC image). Arrows indicate blood vessels surrounding hypoxic region. A high resolution/magnification image showing

nuclear staining of HIF1 α and MLL1 in the hypoxic region is shown in panel b. **(c-d)** DAB staining showing the localization of MLL1 and HIF1 α . Formaldehyde-fixed tumors sections were subjected to DAB staining using MLL1 and HIF1 α antibodies, independently. Nuclear counter staining was done with DAPI.

Author Manuscript

Author Manuscript

Author Manuscript

Author Manuscript